CHIN. PHYS. LETT. Vol. 37, No. 2 (2020) 028103 **Express Letter**

Controlling the Coffee Ring Effect on Graphene and Polymer by Cations *

Haijun Yang(杨海军)[1,4†], Yizhou Yang(杨一舟)[4,5†], Shiqi Sheng(盛世奇)[4], Binghai Wen(闻炳海)[3], Nan Sheng(盛楠)[1,4], Xing Liu(刘星)[2], Rongzheng Wan(万荣正)[1,4], Long Yan(闫隆)[4], Zhengchi Hou(侯铮迟)[1,4], Xiaoling Lei(雷晓玲)[1,4], Guosheng Shi(石国升)[2**], Haiping Fang(方海平)[1,4,5**]

[1]*Shanghai Synchrotron Radiation Facility, Zhangjiang Laboratory (SSRF, ZJLab), Shanghai Advanced Research Institute, Chinese Academy of Sciences, Shanghai 201204*

[2]*Shanghai Applied Radiation Institute and State Key Lab Advanced Special Steel, Shanghai University, Shanghai 200444*

[3]*Guangxi Key Lab of Multisource Information Mining & Security, Guangxi Normal University, Guilin 541004*

[4]*Division of Interfacial Water, CAS Key Laboratory of Interfacial Physics and Technology, Shanghai Institute of Applied Physics, Chinese Academy of Sciences, Shanghai 201800*

[5]*School of Science, East China University of Science and Technology, Shanghai 200237*

(Received 6 January 2020)

Recently, there are great efforts that have been taken to suppressing/controlling the coffee ring effect, but it is of challenge to achieve inexpensive and efficient control with less disturbance, suitable for scalable production and highly enhancing the printing/dyeing color fastness. By only adding trace amounts of salt into the suspensions, here we experimentally achieve the facile and highly efficient control of the coffee ring effect of suspended matter on substrates of graphene, natural graphite, and polyethylene terephthalate surfaces. Notably, friction force measurements show that ion-controlled uniform patterns also greatly enhance color fastness. Molecular dynamics simulations reveal that, due to strong hydrated cation-π interactions between hydrated cations and aromatic rings in the substrate surface, the suspended matters are adsorbed on the surfaces mediated by cations so that the suspended matters are uniformly distributed. These findings will open new avenues for fabricating functional patterns on graphene substrates and will benefit practical applications including printing, coating, and dyeing.

PACS: 81.15.Lm, 81.16.Dn, 68.08.−p DOI: 10.1088/0256-307X/37/2/028103

The coffee ring effect,[1,2] the formation of a ring that occurs when the solvent evaporates from a drop of solution that contains non-volatile solutes in a volatile solvent, has been a large obstacle in many fundamental and daily applications ranging from printing, coating, dyeing, complex assembly, to micro-/nano-fabrication.[3−10] For example, it leads to non-uniform printing and dyeing on polymers and textiles, which greatly affects appearance and product applications. There have been great efforts to suppressing or controlling the effect,[4,5,11−18] such as particle shape variation,[4] addition of surfactants,[11,18−20] polymers,[16] sol-gel inducers,[12] co-solvents,[13,21] or proteins,[14] as well as using external optical or electric fields.[15] These strategies have usually relied on additives,[11−14,16] temperature,[17,22] external optical or electronic fields,[15,18,23] or even making the suspension particle asymmetry.[4,24,25] However, the challenge still remains for inexpensive efficient control, with less disturbance, for scalable production and enhanced color fastness, which are the key to those fundamental and daily applications in a given system.

Fabricating functional patterns on graphene substrates would have great potential applications in many graphene-based fields, such as graphene-based field effect transistors, complex catalysts, nanodevices, and biomolecule detectors.[26−33] Uniform printings/coatings should be an effective pathway for fabricating these functional patterns.[34] Clearly, the ubiquitous nature of the coffee ring effect has made these processes difficult, resulting in inhomogeneous functional patterns.

In this Letter, we experimentally achieve facile and highly efficient control of the coffee ring effect on graphene and polymer surfaces, as well as on other aromatic-ring substrates, simply by adding trace amounts of salt (i.e., NaCl, LiCl, KCl, $CaCl_2$ or $MgCl_2$) to the suspended solute solution. We obtain enhanced color fastness of dye molecules (over 100% for acid red 1). Molecular dynamics (MD) simulations attribute the control to hydrated cation-π interactions between the solute and aromatic rings in the graphene and polymer substrates, promoting adsorption of suspended matters onto the substrates bearing aromatic rings.

In experiment, we used aqueous suspensions of

*Supported by the National Natural Science Foundation of China under Grant Nos. U1632135, U1832170, 11862003, 11474299, 11574339, U1932123, and 11722548, the Key Research Program of Frontier Sciences of the Chinese Academy of Sciences (Nos. QYZDJ-SSW-SLH053 and QYZDJ-SSW-SLH019), and the Key Research Program of the Chinese Academy of Sciences (No. KJZD-EW-M03).

†These authors contributed equally to this work.

**Corresponding author. Email: fanghaiping@sinap.ac.cn; gsshi@shu.edu.cn

polystyrene microspheres, as reported previously.[1,4] Some suspensions were thoroughly mixed with solutions of NaCl to obtain mixtures of different NaCl concentrations. Drops of these mixtures and the aqueous suspensions without NaCl were then placed separately on a chemical vapor deposition (CVD) grown graphene substrate on copper (Fig. 1(a)). After drop evaporation at 10.0 ± 3.2 ℃, the morphologies of the dried patterns left on the substrates were recorded by optical microscopy, followed by a greyscale analysis. Figure 1(b) shows the patterns for the suspension without NaCl. We can see a ring-like pattern with a dark rim and a light grey center on graphene, which displays a clear coffee ring effect. Remarkably, as shown in Figs. 1(c)–1(e), the image contrast between the rim and center of the pattern was gradually reduced for mixtures with increasing NaCl concentration (2.0–8.0 mM). In fact, at the concentration of 8.0-mM NaCl, the pattern in Fig. 1(e) appears to be uniform. Other salts such as LiCl, KCl, $CaCl_2$, and $MgCl_2$, were also effective (Figs. S4–S7).

Notably, the ionic control behavior was also observed on other substrates such as the most common thermoplastic polymer resin of polyethylene terephthalate (PET) and natural graphite surfaces (Figs. S8–S11). As shown in Fig. 1(g), the ring-like feature on a PET film disappeared at the NaCl concentration of 16 mM. In the depicted studies, we used aqueous soluble acid red 1 and acid blue 25 dye molecules, respectively.

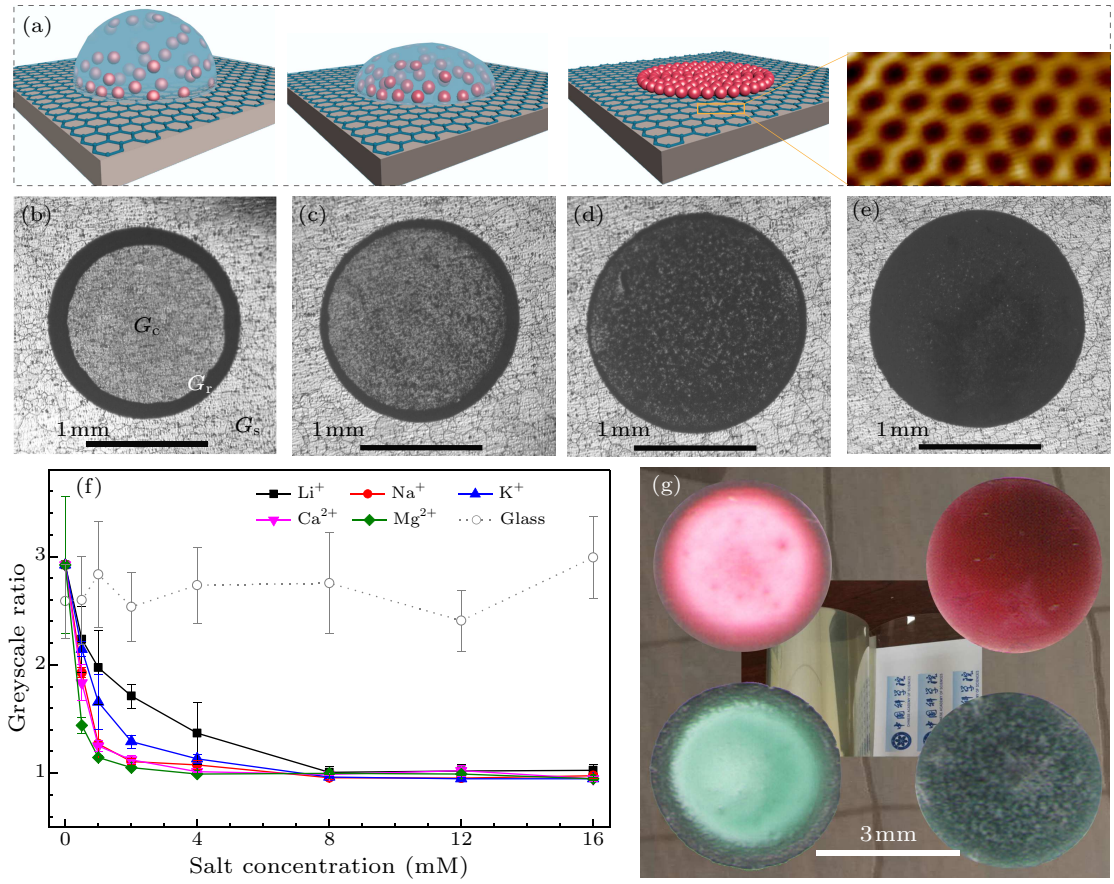

Fig. 1. Control of the deposition patterns of suspended matters by cations. (a) A schematic of how cations in a drop (blue hemisphere) determine the deposition of polystyrene microspheres (red beads). The inset shows an atomically resolved scanning tunneling microscopy (STM) image of a graphene lattice. (b)–(e) Optical microscopy images of particle patterns on graphene after evaporation of drops of suspension or mixture with different salt concentrations (0 mM, 2.0 mM, 4.0 mM, and 8.0 mM, respectively). (f) Greyscale ratios ($\mathrm{GR} = \frac{G_c - G_s}{G_r - G_s}$) of patterns of the deposited matters on graphene (solid lines) and glass (dotted line) substrate. (g) Photographs of patterns on a PET film after evaporation of drops of mixtures of acid red 1 (upper) and acid blue 25 (lower) solutions with 0 mM (left) and 16.0 mM (right) NaCl, respectively.

To quantitatively characterize the uniformity of the deposited polystyrene microspheres, we computed the greyscale ratio, denoted by GR, $\mathrm{GR} = (G_c - G_s)/(G_r - G_s)$, where G_c, G_r, and G_s are the average greyscales at the pattern center, the pattern rim, and the substrate, respectively. As shown in Fig. 1(f), the greyscale ratio greatly decreases from 2.90 ± 0.72 for the suspension without NaCl to 1.00 ± 0.05 for the mixture with 8.0 mM NaCl solution. It is clear that GR = 1.00 corresponds to uniform deposition. Thus,

the pattern was essentially uniform at the salt concentration equal to and greater than 8.0 mM. These results clearly indicate that the ring-like pattern can be well controlled by the concentration of NaCl in the mixture.

Values of GR using other salts (i.e., LiCl, KCl, $CaCl_2$, and $MgCl_2$) showed that patterns approached uniformity at 8.0 mM and 4.0 mM for monovalent and divalent cations, respectively, although their decreasing ratios of GR values differed (Fig. 1(f)). In particular, the GR ratio decreased more slowly for drops mixed with monovalent cations than that with divalent cations.

The ion-controlled uniform patterns clearly enhanced the color fastness of the dye molecules. This was demonstrated via contact atomic force microscopy (AFM, Figs. S12–S14). Specifically, we measured friction forces while scanning four dye patterns formed after evaporation. As shown in Fig. S14, the friction forces of coral red and dark cyan dye patterns reach 220.0 ± 67.0 nN and 79.6 ± 14.8 nN, respectively, at the NaCl concentration of 16.0 mM. These values were factors of 2.14 and 1.24 greater, respectively, than those measured for patterns produced without NaCl.

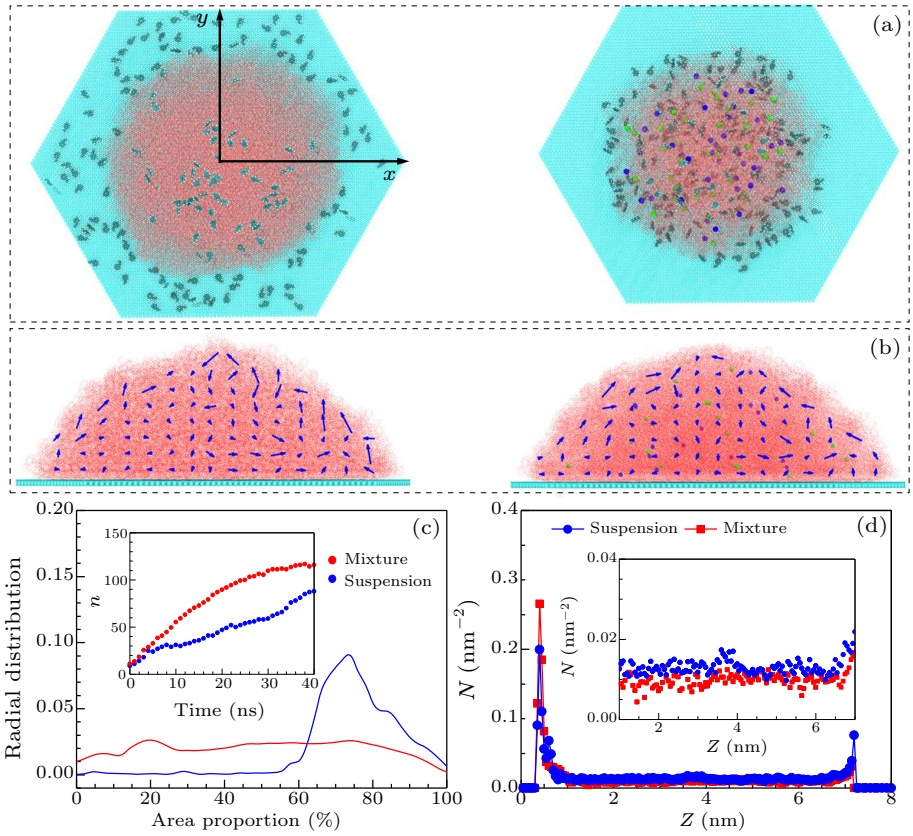

Fig. 2. Molecular dynamic simulations of the styrene molecules in drops of suspension or mixture on graphene sheets. (a) Top views of the drops of suspension and mixture on graphene during evaporation. The cyan, red, blue, green, and white spheres represent C, O, Na, Cl, H atoms, respectively. (b) Flow rate distributions in drop suspensions (without NaCl, left) or mixtures (with NaCl, right). (c) Radial distribution for the first layer (<1 nm) of styrene molecules from the center of the drops. The inset plots the number n of styrene molecules adsorbed on the surface (n) with time. (d) Density distribution of styrene molecules per square (N) along the Z direction in the drops of suspension (blue) or mixture (red).

We performed MD simulations to exploit the underlying physics. We used styrene molecules as the suspensions and a graphene sheet with aromatic rings as the solid surface since the polystyrene microspheres were too large to perform MD simulations. In the system without salt, most of the styrene molecules formed a ring-like pattern on the graphene surface around the drop of the aqueous suspension as the water evaporated. In contrast, most of the styrene molecules with 0.1 M NaCl spread out on the graphene surface as the water evaporated (Fig. 2(a)). The inset of Fig. 2(c) shows that most of the styrene molecules are adsorbed on the surface after 40 ns simulation in both systems, and the height of these adsorbed styrene molecules is below 1 nm (Fig. 2(d)). The radial distribution of these adsorbed styrene molecules is shown in Fig. 2(c). It was flat in the presence of NaCl, and displayed a peak near the edge of the drop in its absence, which is consistent with our experimental observations. We also computed the distribution of flow

rates in the drop (Fig. 2(b)). The liquid flow displayed loops. For suspensions without cations, the flow loop pushed the styrene molecules to the drop boundary. Thus, sedimentation was greater at the boundary. In contrast, for mixtures with cations, due to the strong hydrated cation-π interactions between the hydrated cations and aromatic rings structures in the surfaces, the styrene molecules were adsorbed onto the graphene by the cations. The adsorbed styrene molecules were not further disturbed by the flow loops toward the drop boundary, consistent with the lattice Boltzmann simulation and the *in situ* experiments (Figs. S15 and S16).

To further investigate the importance of hydrated cation-π interactions between the salt and the substrate in the suppression of coffee rings, we have performed experiments at the same NaCl concentration and only replaced the substrate with a glass slide that does not contain any aromatic rings. Considering that there are no hydrated cation-π interactions between the salt and the substrate, we expected that the ring-like morphology would still exist. This was borne out in the experiments (Fig. 1(f) and Fig. S17).

In summary, we have experimentally achieved facile and precise control of deposition patterns of suspended particles and molecules on graphene and other substrates bearing aromatic rings by adding trace amounts of salt to the suspensions. The ion-controlled uniform patterns greatly enhanced color fastness as well, i.e., over 100% for acid red 1. The physics underlying this process may be mainly attributed to the strong hydrated cation-π interactions between the hydrated cations and the aromatic rings on the substrates surface. The suspended matter is uniformly adsorbed on the surfaces mediated by cations and are not further perturbed by flow loops to the drop boundary. In addition to Na^+, other metal ions could be used to control the particle deposition on substrate surfaces with aromatic rings where cation-π interactions occur.[35–40] Overall, our findings represent a step towards a wide range of applications involving evaporation and fabrication of functional patterns on graphene as well as on other aromatic-ring-containing substrates. Examples include packaging, high-temperature fuel cells, thin-film solar cells, displays, textiles, electronics, and military applications.

References

[1] Deegan R D, Bakajin O, Dupont T F et al 1997 *Nature* **389** 827
[2] Larson R G 2017 *Nature* **550** 466
[3] Minemawari H, Yamada T, Matsui H et al 2011 *Nature* **475** 364
[4] Yunker P J, Still T, Lohr M A et al 2011 *Nature* **476** 308
[5] 2014 *Nature* **515** 166
[6] Han W and Lin Z 2012 *Angew. Chem. Int. Ed.* **51** 1534
[7] Zhang Z, Zhang X, Xin Z et al 2013 *Adv. Mater.* **25** 6714
[8] Diao Y, Tee B C K, Giri G et al 2013 *Nat. Mater.* **12** 665
[9] Devineau S, Anyfantakis M, Marichal L et al 2016 *J. Am. Chem. Soc.* **138** 11623
[10] Liu G L, Kim J, Lu Y et al 2006 *Nat. Mater.* **5** 27
[11] Sempels W, De Dier R, Mizuno H et al 2013 *Nat. Commun.* **4** 1757
[12] Talbot E L, Yang L, Berson A et al 2014 *ACS Appl. Mater. & Interfaces* **6** 9572
[13] Bail R, Hong J Y and Chin B D 2018 *RSC Adv.* **8** 11191
[14] Gorr H M, Zueger J M and Barnard J A 2012 *J. Phys. Chem. B* **116** 12213
[15] Lei Y, Zhang X, Xu D et al 2018 *J. Phys. Chem. Lett.* **9** 2380
[16] Cui L, Zhang J, Zhang X et al 2012 *ACS Appl. Mater. & Interfaces* **4** 2775
[17] Li Y, Yang Q, Li M et al 2016 *Sci. Rep.* **6** 24628
[18] Manos A and Damien B 2014 *Angew. Chem. Int. Ed.* **53** 14077
[19] Seo C, Jang D, Chae J et al 2017 *Sci. Rep.* **7** 500
[20] Anyfantakis M, Geng Z, Morel M et al 2015 *Langmuir* **31** 4113
[21] Tekin E, De Gans B J and Schubert U S 2004 *J. Mater. Chem.* **14** 2627
[22] Soltman D and Subramanian V 2008 *Langmuir* **24** 2224
[23] Yen T M, Fu X, Wei T et al 2018 *Sci. Rep.* **8** 3157
[24] Dugyala V R and Basavaraj M G 2014 *Langmuir* **30** 8680
[25] Larson R G 2012 *Angew. Chem. Int. Ed.* **51** 2546
[26] Liu L H , Zorn G, Castner D G et al 2010 *J. Mater. Chem.* **20** 5041
[27] Shuping P, Yenny H, Xinliang F et al 2011 *Adv. Mater.* **23** 2779
[28] Novoselov K S, Fal'ko V I, Colombo L et al 2012 *Nature* **490** 192
[29] Esfandiar A, Radha B, Wang F C et al 2017 *Science* **358** 511
[30] Jain T, Rasera B C, Guerrero R J S et al 2015 *Nat. Nanotechnol.* **10** 1053
[31] Wu X, Pei Y and Zeng X C 2009 *Nano Lett.* **9** 1577
[32] Stankovich S, Dikin D A, Dommett G H B et al 2006 *Nature* **442** 282
[33] Yasaei P, Kumar B, Hantehzadeh R et al 2014 *Nat. Commun.* **5** 4911
[34] Secor E B, Lim S, Zhang H et al 2014 *Adv. Mater.* **26** 4533
[35] Shi G, Chen L, Yang Y et al 2018 *Nat. Chem.* **10** 776
[36] Chen L, Shi G, Shen J et al 2017 *Nature* **550** 380
[37] Shi G, Liu J, Wang C et al 2013 *Sci. Rep.* **3** 3436
[38] Ma J C and Dougherty D A 1997 *Chem. Rev.* **97** 1303
[39] Mahadevi A S and Sastry G N 2013 *Chem. Rev.* **113** 2100
[40] Shi G, Dang Y, Pan T et al 2016 *Phys. Rev. Lett.* **117** 238102

Supplementary Material: Controlling the coffee ring effect on graphene and polymer by cations*

Haijun Yang (杨海军)[1,4]†, Yizhou Yang(杨一舟)[4,5]†, Shiqi Sheng(盛世奇)[4], Binghai Wen(闻炳海)[3], Nan Sheng(盛楠)[1,4], Xing Liu(刘星)[2], Rongzheng Wan(万荣正)[1,4], Long Yan(闫隆)[4], Zhengchi Hou(侯铮迟)[1,4], Xiaoling Lei(雷晓玲)[1,4], Guosheng Shi(石国升)[2]**, Haiping Fang(方海平)[1,4,5]**

[1] Shanghai Synchrotron Radiation Facility, Zhangjiang Laboratory (SSRF, ZJLab), Shanghai Advanced Research Institute, Chinese Academy of Sciences, Shanghai, 201204, China

[2] Shanghai Applied Radiation Institute and State Key Lab Advanced Special Steel, Shanghai University, Shanghai 200444, China

[3] Guangxi Key Lab of Multisource Information Mining & Security, Guangxi Normal University, Guilin 541004, China

[4] Division of Interfacial Water, CAS Key Laboratory of Interfacial Physics and Technology, Shanghai Institute of Applied Physics, Chinese Academy of Sciences, Shanghai 201800, China

[5] School of science, East China University of Science and Technology, Shanghai 200237, China

*Supported by the National Natural Science Foundation of China under Grant Nos (U1632135, U1832170, 11862003, 11474299, 11574339, U1932123, and 11722548), the Key Research Program of Frontier Sciences of the Chinese Academy of Sciences (No. QYZDJ-SSW-SLH053 and QYZDJ-SSW-SLH019), the Key Research Program of the Chinese Academy of Sciences (No. KJZD-EW-M03)

†These authors contributed equally to this work

**Email: fanghaiping@sinap.ac.cn; gsshi@shu.edu.cn

Text A: Materials

Ultrapure water (Milli-Q, Millipore, 18.2 MΩ·cm resistivity) was used for all experiments. The monodisperse polystyrene microspheres suspension (diameter: 1 μm, 1% w/v) was purchased from Shanghai So-Fe Biomedicine Company, centrifuged, washed, and redispersed into pure water before use. Graphene monolayer (300 mm*245 mm, monolayer coverage >99%) were manufactured by Chongqing Graphene Technology Company through CVD method on copper foil. Graphites (HOPG, grade ZYB type) were purchased from Shanghai NTI Co., Ltd. Sodium chloride (NaCl) and lithium chloride (LiCl) of AR grade were provided by Sinopharm

Chemical Reagent Company. Polyethylene terephthalate (PET) films were produced by Shanghai Zicheng Packaging Materials Company. Dyes (Acid Red 1 and Acid Blue 25) were kindly provided by Winchem Industrial Company. All the substrates, the salts, and the dyes were used as received.

Text B: Experimental setup for drying drops

The 0.146 g of NaCl was dissolved into 10 ml ultrapure water to prepare the aqueous solution at the concentration of 0.25 M. Then, twice echelon dilution was used to get a serial of concentrations. 100 μl of polystyrene suspension and 100 μl of salt solution with different concentrations were added into an Eppendorf tube, reciprocatingly sucked with a micropipette (Eppendorf), and vortexed for 1 min to thoroughly mix them together. A drop (0.4 μl) of the as prepared mixture was then immediately deposited onto the graphene substrate in a petri dish by using a micropipette, loosely covered to avoid air currents or contaminants in the environment. The deposition of other saline mixture drops with KCl, LiCl, $MgCl_2$, or $CaCl_2$ followed the same procedure. The temperature for drying was 10 ± 3.2 ℃, with the relative humidity of ~45 ± 7.3%. In order to clearly view the deposition of polystyrene microspheres or dyes (0.05 M) on PET with naked eye, the drop volume of mixture was 100 μl. As a control, ultrapure water with the same volume as the salt solution was added to mix with the polystyrene suspension or dye solutions following the same procedure in all experiments.

Text C: Imaging of the deposits

Reflected brightfield greyscale images of the deposited patterns were captured using an optical microscopy (Axio Imager.M2m, Zeiss). All images were acquired in similar illumination conditions and acquisition settings. They are displayed without any postprocessing.

Text D: Greyscale analysis of the deposited pattern structures

First, we obtained the gray-level values of all pixels for each photo. Then, from the center of circle, the gray-level values were collected in four directions ($+x$, $-x$, $+y$, $-y$) with respect to the distance away from the center. Here, we run average over 100 pixels in width. As the gray-level values apparently jumped at the edge region, the gray-level values were divided into three regions, including the center (G_c), the rim (G_r), and the substrate (G_s).

Text E: Friction measurement on the deposited dye layers

All AFM experiments were performed using a Multimode-8 AFM with Nanoscope V controller and J scanner (Bruker, Santa Barbara, CA, USA). AFM cantilevers (XSC11 Al/BS) were purchased from MikroMasch, Tallinn, Estonia. This Rectangular cantilevers with nominal spring constants of 42 N/m were used to scratch the

deposited dye layer. Its nominal thickness, tip height, cantilever length, and cantilever width are 2.7 μm, 15 μm, 100 μm, and 50 μm, respectively. All operations were performed in an environmental chamber (Shanghai Espec Environmental Equipment Corporation) under a relative humidity of ~30% and at a temperature of ~24 ℃.

In a friction measurement, height images and friction signal images in both the trace and retrace directions were collected simultaneously at a scan angle of 90 ° (i.e. orthogonal to the long axis of the cantilever) [1], as shown in Fig. S1. The friction hysteresis at a given sample position can be calculated by subtracting the retrace frictional signal images from the trace one, is considered to be twice of the friction force exerted at that point.[2] The height images were chosen to inspect the damage of the scanned area by comparing the topography change of two adjacent images scanned under a rising "deflection setpoint". As shown in Fig. S11, the crack scanned at the deflection setpoint of 3.0 V is clearly wider than that scanned at 2.5 V, indicating that the highest friction force that the deposited layer can endure is about 3.0 V. Then the friction hysteresis was calculated, followed by a 'section analysis' along its *x*-direction to get a friction profile at this position. The baseline was extracted from this friction profile, and recorded as half ot the friction forces at this position.[2] We repeated 8 times at different places near the peripheral of the deposited layer for each sample, following a statistical analysis. But the friction force (V_{lateral}) takes mV as unit now.

To transfer the unit of V_{lateral} from mV to nN, the lateral sensitivity of the photodetector of the AFM system (S_{lateral}) and the lateral spring constant of the cantilever (k_{lateral}) should be determined. The S_{lateral} is the slope of the friction-lateral displacement curve (42.2 ± 1.35 mV/nm, shown in Fig. S12). The k_{lateral} can be simply calculated from the shape of AFM tip, via: [1, 3]

$$k_{lateral} = \frac{Gwt^3}{3L\left(h+\frac{t}{2}\right)^2}, \quad (1)$$

where *G*, *w*, *t*, *L*, and *h* is the shear modules, width, thickness, length, and height of the AFM tip, respectively. The friction force in nN (F_{lateral}) then can be calculated by:[1]

$$F_{lateral} = \frac{k_{lateral}}{S_{lateral}} V_{lateral}, \quad (2)$$

Text F: Theoretical computational methods

MD simulations were performed using a time step of 1.0 fs with NAMD 2.10 [5] in an NVT [6, 7], ensemble with a time step of 1.0 fs. Each simulation system has an initial size of 60 nm×60 nm×120 nm. Langevin thermostat was applied every 0.5ps to keep the system at 350 K. The carbon atoms of graphene were fixed. An accelerating region was applied from 9.0 nm to 10 nm above the graphene. When a water molecule runs into the accelerating region, an upward force of 1.0 kcal mol^{-1} $Å^{-1}$ (force vector (0, 0, 1)) was applied to the oxygen atom to prevent the water molecule from going back to the graphene surface. This nonequilibrium condition is equivalent to the settings used in other literature reports [8-10], in which evaporated molecules run into an infinite vacuum.

In the classic MD simulations, there are two systems of the styrene molecules in pure water and NaCl solution on a graphene sheet with 7574 carbon atoms. Both of them have the same numbers of 192 styrene molecules. The mixture with NaCl concentrations of 0.1 M contains 19714 water molecules and 40 Na^+ and 40 Cl^- ions. The system without the salt contains 19794 water molecules. Carbon atoms were modeled with a cross-section of σ_{CC}= 3.55 Å and a depth of the potential well of ε_{CC} = -0.070 kcal mol^{-1}. Na^+ and Cl^- ions were assigned to have charges of 1.0 e and -1.0 e, respectively, with Lennard-Jones parameters of σ_{NaNa} = 2.43 Å, σ_{ClCl} = 4.04 Å, ε_{NaNa} = -0.047 kcal mol^{-1} and ε_{ClCl} = -0.150 kcal mol^{-1}. The water model of SPC/E is employed. All of parameters including above lists were derived from the CHARMM force field. The particle-mesh Ewald method [11] with a real space cutoff of 10 Å was used to treat long-range electrostatic interactions and 10 Å cutoff was applied to the van der Waals interactions. According to our previous work [12], we used the TclBC interface to incorporate the cation-π interaction between ions and graphitic surface in NAMD software.

Text G: Simulation of Particles Deposition in Evaporating Droplet by Lattice Boltzmann Method

The simulation is performed by the chemical-potential-based multiphase flow model, which is driven by chemical potential on the single-relaxation-time lattice Boltzmann method [13]. The model uses equation of state (EOS) to control phase transition and fully meets thermodynamics and Galilean invariance. In the present simulations, the flow field is a cuboid, whose length, width and height are 120, 120 and 100-lattice units, respectively. The Peng-Robinson EOS is selected to model the water/vapor system. The periodic boundary condition is applied on the front, back, left and right boundaries. The halfway bounce-back and open boundary conditions are applied on the top boundary before and after 10000 time steps, respectively. The chemical-potential boundary condition is applied on the bottom boundary[14]. The center part with the radius 50- latttice units of the bottom boundary is hydrophilic, and the other part is hydrophobic. The initial liquid phase is a hemisphere with the radius 50-lattice units locating on the hydrophilic part. Initially, 100 spherical particles with the radius 2.6 lattice units are randomly distributed in the drop. The particle surface has neutral wettability when the liquid is pure water. If NaCl or LiCl is dissolved into the water, the chemical potential of the particle surface is relatively brought down. The particles suspend and move with the flow of the water. The hydrodynamic forces exerted on the particles are evaluated by Galilean-invariant momentum exchange method [15]. If a particle is less than 0.1-lattice unit from the baseplate and its velocity is less than 0.01, it is considered to be adsorbed on the baseplate. The initial temperature of the flow field is 0.8 and the temperature of the baseplate is 0.85. After 10000 time steps at which the drop almost reaches its equilibrium state, the temperature begins to evolve according to the standard diffusion-advection equation [16]. With the increase of the drop temperature, the liquid drop evaporates and carries the particles to move.

Figure S1: Schematic of the frictional measurement using an AFM tip on a deposited layer. The pink pancake presents the deposited dyes layer. PSPD is a position sensitive photodetector. In a typical measurement, an AFM tip is in close contact with the sample, scanning and rubbing the deposited layer in a direction orthogonal to the long axis of the cantilever. The friction between the sample and the tip leads to torsion of the cantilever and a lateral voltage signal ($V_{lateral}$).

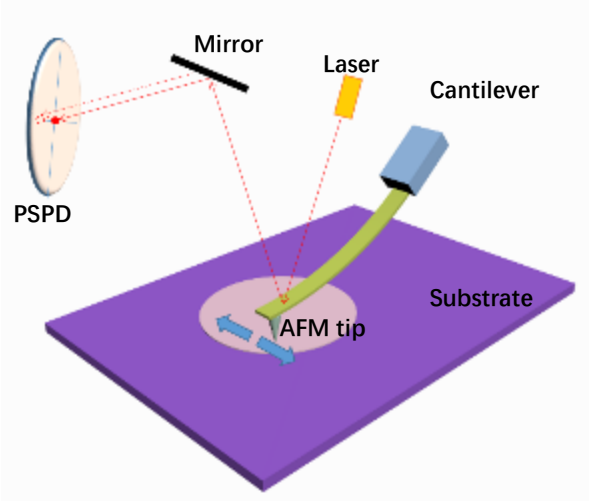

Figure S2: Snapshots of the initial system models of the styrene molecules in NaCl solution (a) and pure water (b) on a graphene sheet, respectively. Spheres in cyan, white, and red represent carbon, hydrogen and oxygen atoms. Blue and green spheres represent Na^+ and Cl^-. (c) Radical distribution of styrene molecules with the distance on the graphene sheet.

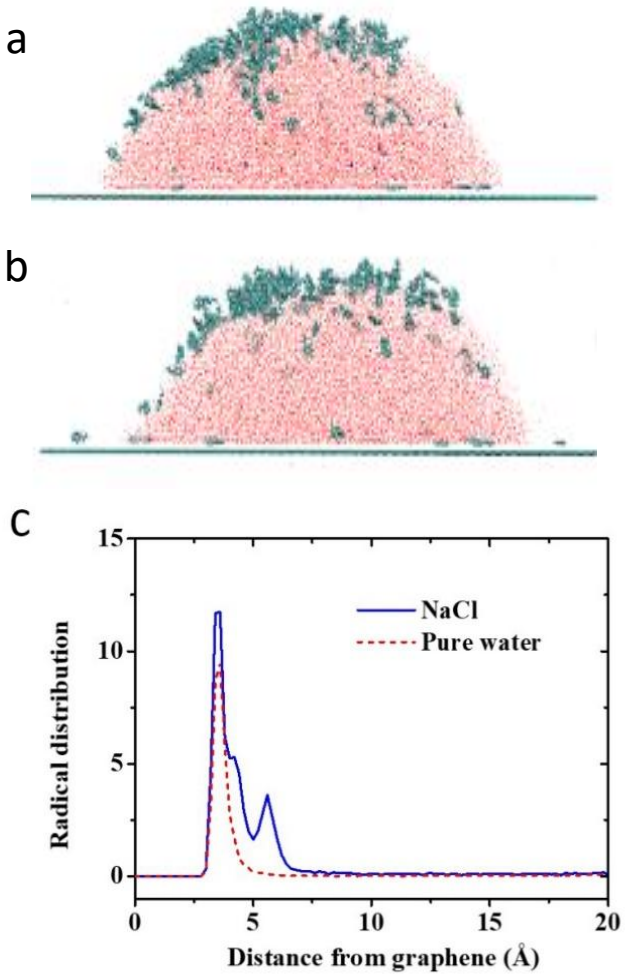

Figure S3: Photograph of a graphene substrate grown on copper foil by chemical vapor deposition (CVD). It is manufactured by Chongqing Graphene Technology Company. The coverage of graphene monolayer is larger than 99%.

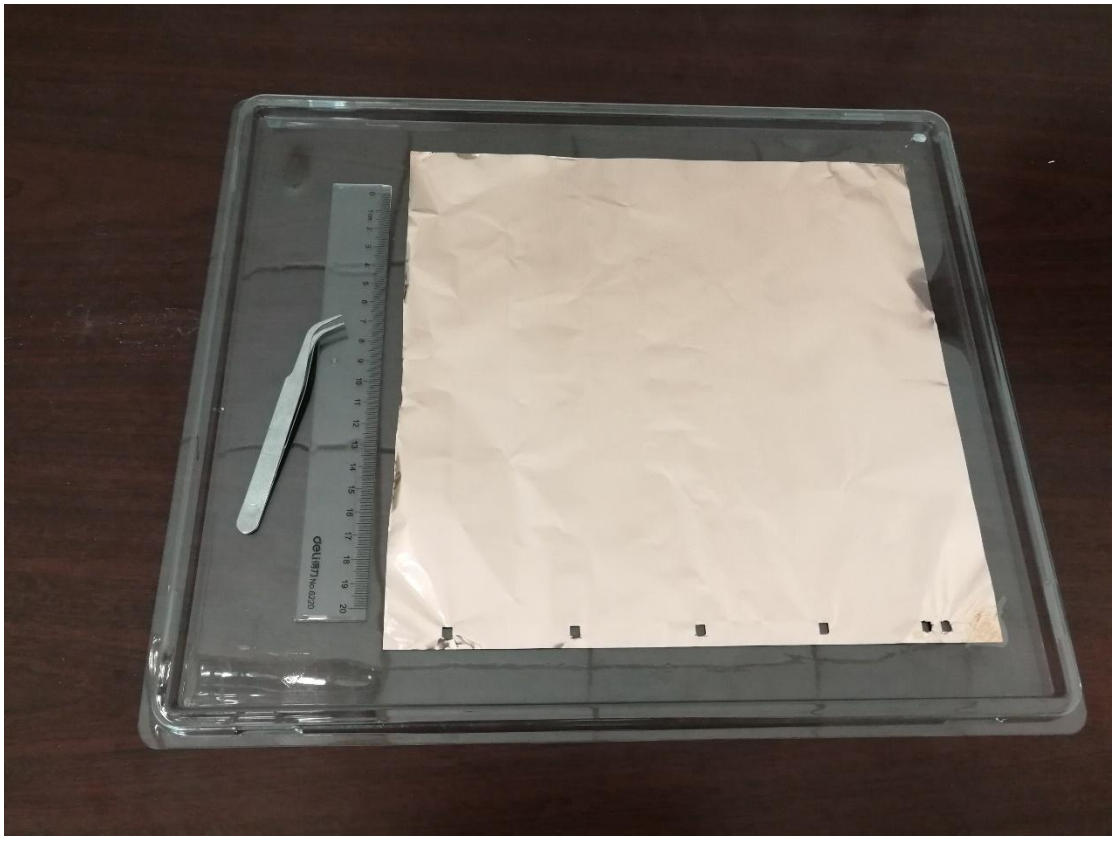

Figure S4: Deposited patterns of a drop of polystyrene microspheres with different LiCl concentrations after evaporation on graphene. a, 0 mM. b, 2.0 mM, c, 4.0 mM, d, 8.0 mM, e, 16 mM. Scale bars: 1mm. We can see a ring-like pattern with a dark rim and a light grey center on graphene, which displays a clear coffee ring effect. Remarkably, as shown in Fig. S4b – S4d, the image contrast between the rim and the center of the pattern is gradually reduced for the mixture with the LiCl concentration increasing from 2.0 mM to 8.0 mM.

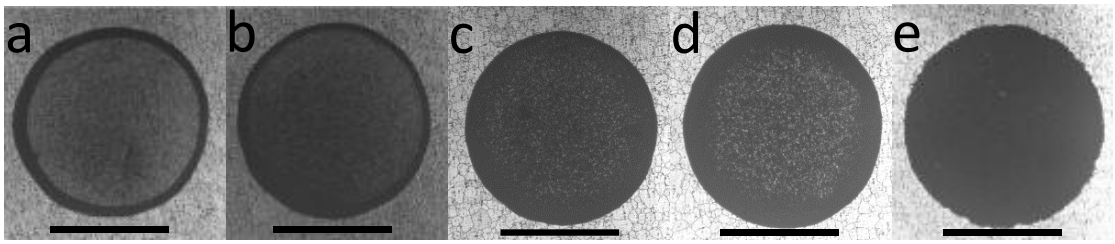

Figure S5: Deposited patterns of a drop of polystyrene microspheres with different KCl concentrations after evaporation on graphene. a, 0 mM. b, 2.0 mM, c, 4.0 mM, d, 8.0 mM, e, 16 mM. Scale bars: 1mm. The image contrast between the rim and the center of the pattern is gradually reduced for the mixture with the KCl concentration increasing from 1.0 mM to 8.0 mM. In fact, at the concentration of 8.0 mM, the pattern looks like a uniform black pancake.

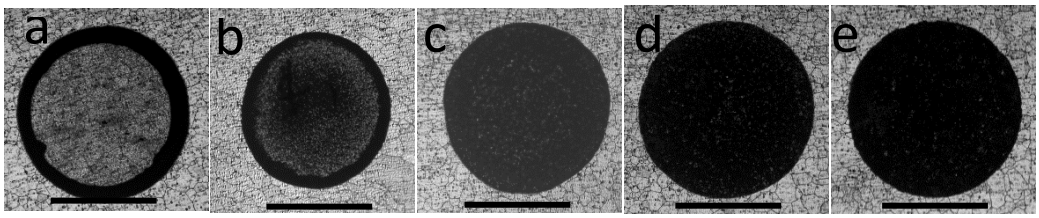

Figure S6: Optical microscopy images of polystyrene microspheres patterns deposited at different $CaCl_2$ concentration in the droplet. a, 0.5 mM, b, 1.0 mM, c, 2.0 mM, d, 4.0 mM, e, 8.0 mM, f, 12 mM. Scale bars: 1 mm. The image contrast between the rim and the center of the pattern is gradually reduced for the mixture with the $CaCl_2$ concentration increasing from 0.5 mM to 4.0 mM. In fact, at the concentration of 4.0 mM, the pattern looks like a uniform black pancake.

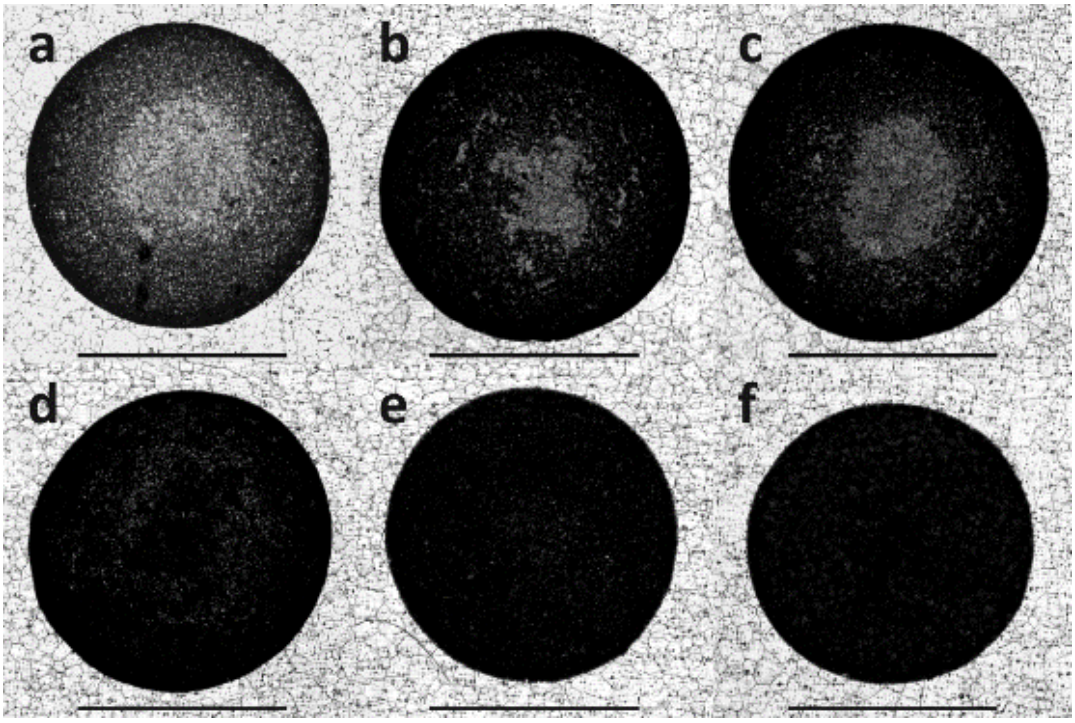

Figure S7: Optical microscopy images of polystyrene microspheres patterns deposited at different $CaCl_2$ concentration in the droplet. a, 0.5 mM, b, 1.0 mM, c, 2.0 mM, d, 4.0 mM, e, 8.0 mM, f, 12 mM. Scale bars: 1 mm.The image contrast between the rim and the center of the pattern is gradually reduced for the mixture with the $MgCl_2$ concentration increasing from 0.5 mM to 4.0 mM. In fact, at the concentration of 4.0 mM, the pattern looks like a uniform black pancake.

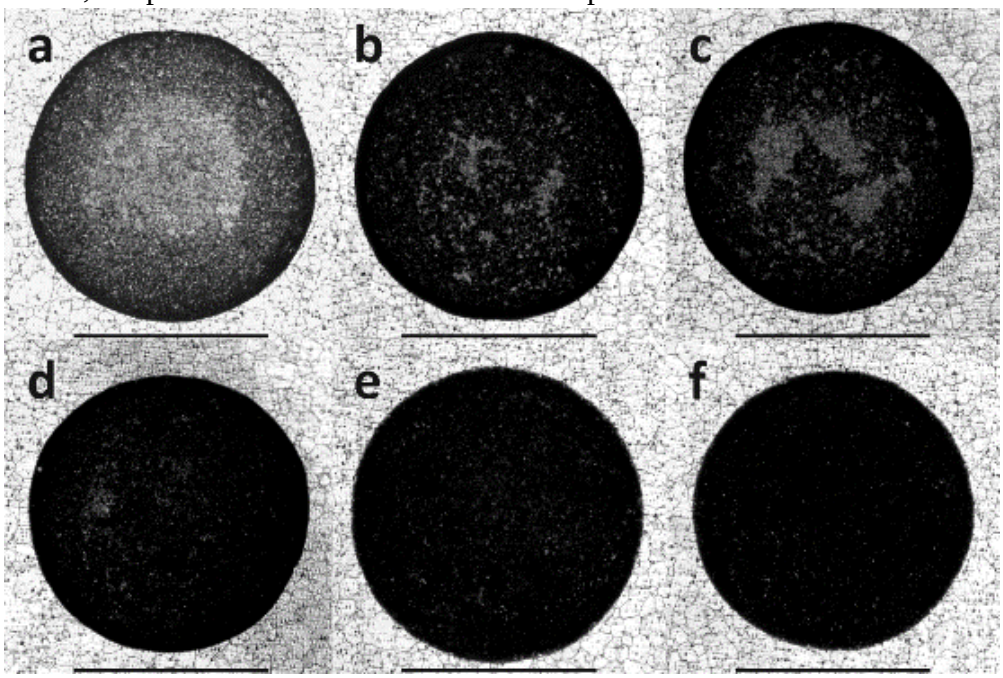

Figure S8: Deposited patterns from a drop of polystyrene microspheres with different NaCl concentrations after evaporation on PET (Polyethylene terephthalate). Left: 0 mM, right: 8.0 mM. The deposited polystyrene microspheres form a ring-like pattern on PET films at the absence of ions in the suspension, clearly showing the typical coffee ring effect. At the NaCl concentration of 8.0 mM, a uniform white pancake appears due to the suppression of the coffee ring effect by the trace amount of ions in the mixture.

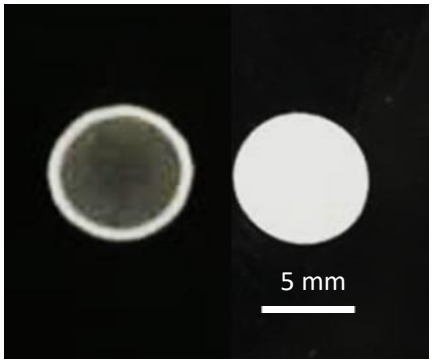

Figure S9: Deposited patterns of a drop of polystyrene microspheres containing different NaCl concentrations after evaporation on graphite. a, 0 mM, b, 2.0 mM, c, 4.0 mM, d, 8.0 mM, e, 16 mM. The dot line represents the initial boundary of the droplet, and the arrows displays the move direction of the contact line between the droplet and graphite. Scale bars: 2 mm.

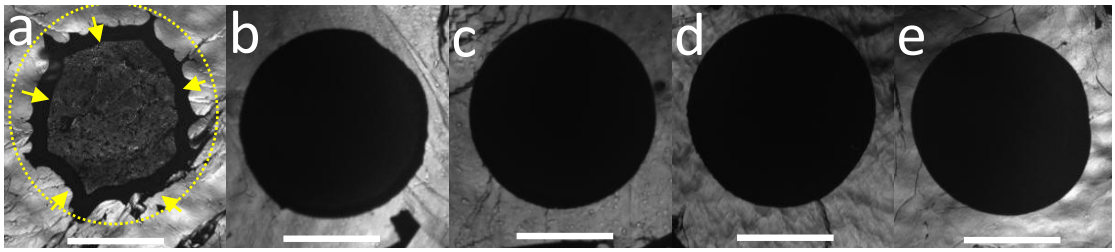

Figure S10: SEM images of polystyrene microspheres patterns on graphite deposited from suspension or mixture with Na^+ concentration of (a), 0 mM, and (b), 16 mM. The insets are the zoom-in images of the selected area at the rim or the center of the deposit. Scale bar: 10 μm.

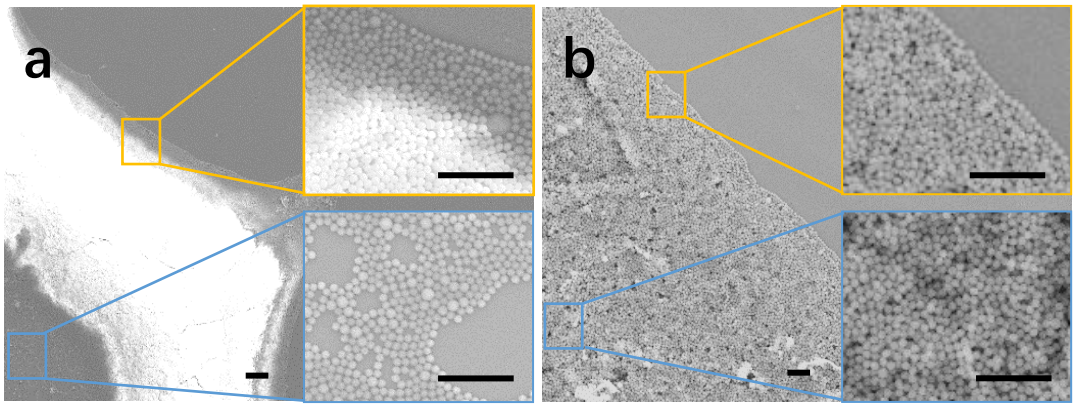

Figure S11: Molecular structures of (a), PET, (b), Acid Red 1, and (c), Acid Blue 25.

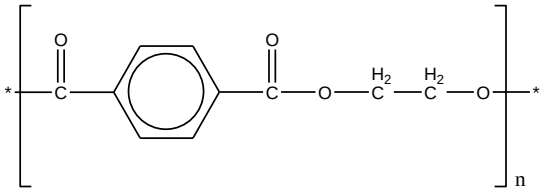

(a)

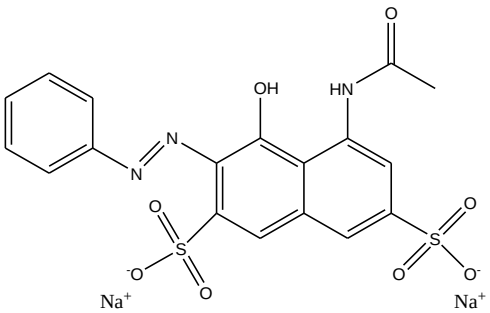

(b)

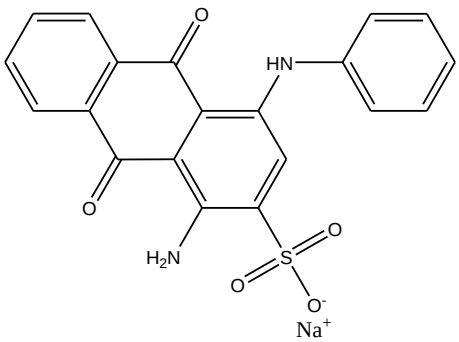

(c)

Figure S12: *In situ* AFM height images of Acid blue 25 layer deposited without NaCl scanned at a rising 'deflection setpoint'. a, 2.0 V, b, 2.5 V, c, 3.0 V (first scan), d, 3.0 V (second scan), e, 3.0 V (third scan). The deposited layer is stable under friction with the 'deflection setpoint' of 2.5 V. Further increase of the 'deflection setpoint' to 3.0 V leads to the formation of a rupture at the bottom left corner of the scan area (displayed in Fig. S12c). Continuous scanning at the same position gradually enlarges the rupture (Fig. S12d – S12e). Thus, we deemed that 3.0 V would be the critical 'deflection setpoint' to damage the deposited layer. And the baseline of the section profile of its corresponding friction hysteresis image is extracted to statistically analyze the critical friction force ($V_{lateral}$).

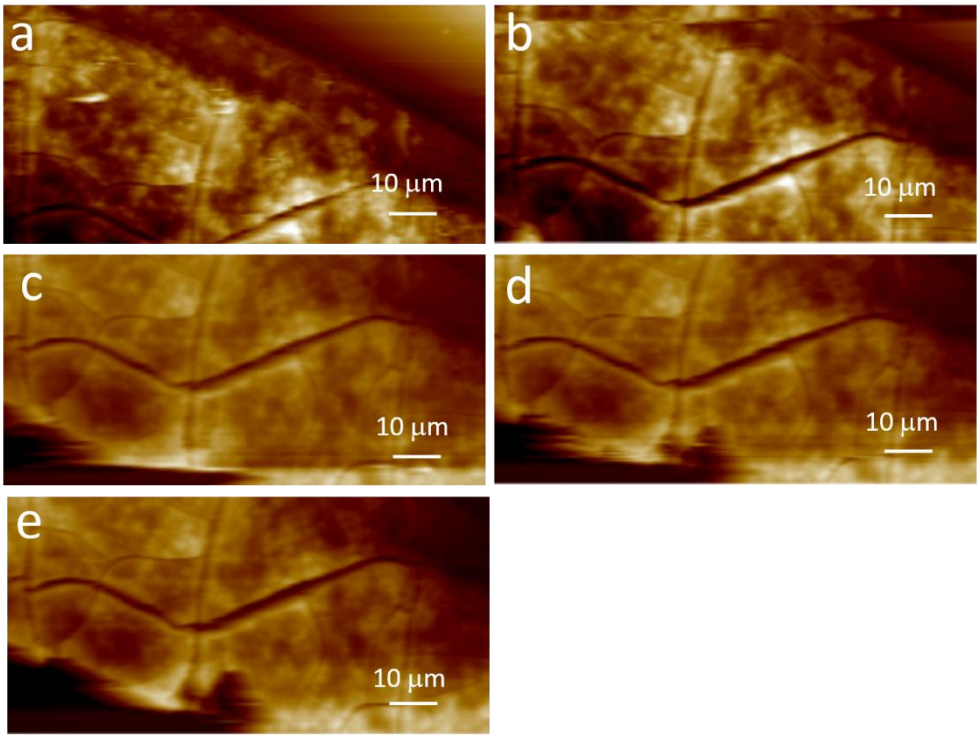

Figure S13: Friction-lateral displacement curve for the calibration of the lateral sensitivity of the photodetector of the AFM system ($S_{lateral}$). The slop of the curve at the first 2 nm of the lateral displacement is 42.2 ± 1.35 mV/nm—that's the $S_{lateral}$.[1]

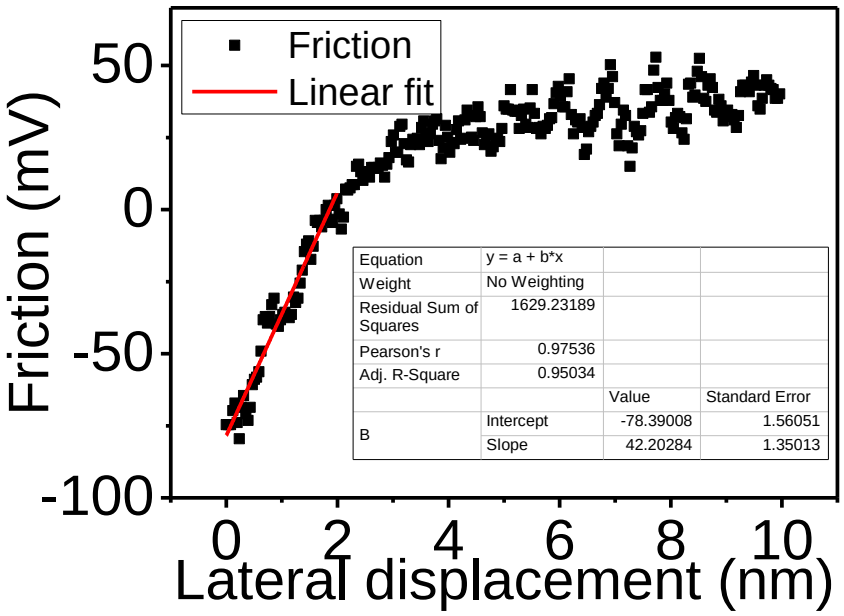

Figure S14: Friction force of deposited dye patterns on polyethylene terephthalate (PET) films from drops with different salt concentration. It indicates that the ion-controlled uniform patterns clearly enhanced the color fastness of the dye molecules.

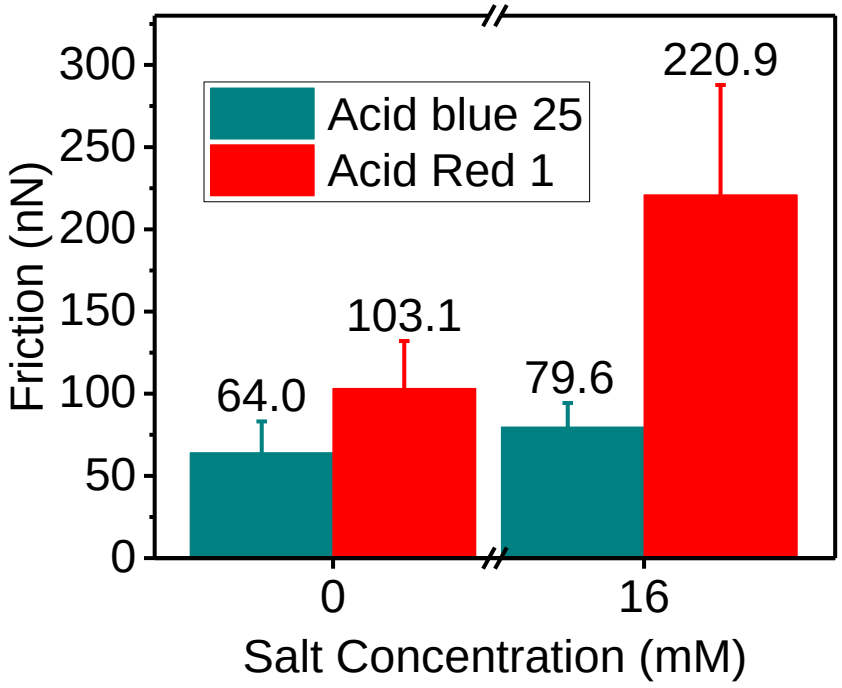

Figure S15. LBM Snapshots for drops of suspension (a) and mixture (b) before (Left) and after (Right) evaporation, respectively. Red liquid represents water, while cyan spherules represent particles. Most of the adsorbed cyan spherules were on the rim and form a ring-like pattern, which displays a clear coffee ring effect in the absence of cations for the suspension drop. In contrast, the adsorbed cyan spherules spread over the contact area between the drop and the substrate in the presence of NaCl in the mixture drop. In a word, all of these results clearly indicate that the ring-like pattern can be well controlled by NaCl in the mixture drop, consistent with our experiments and MD simulations.

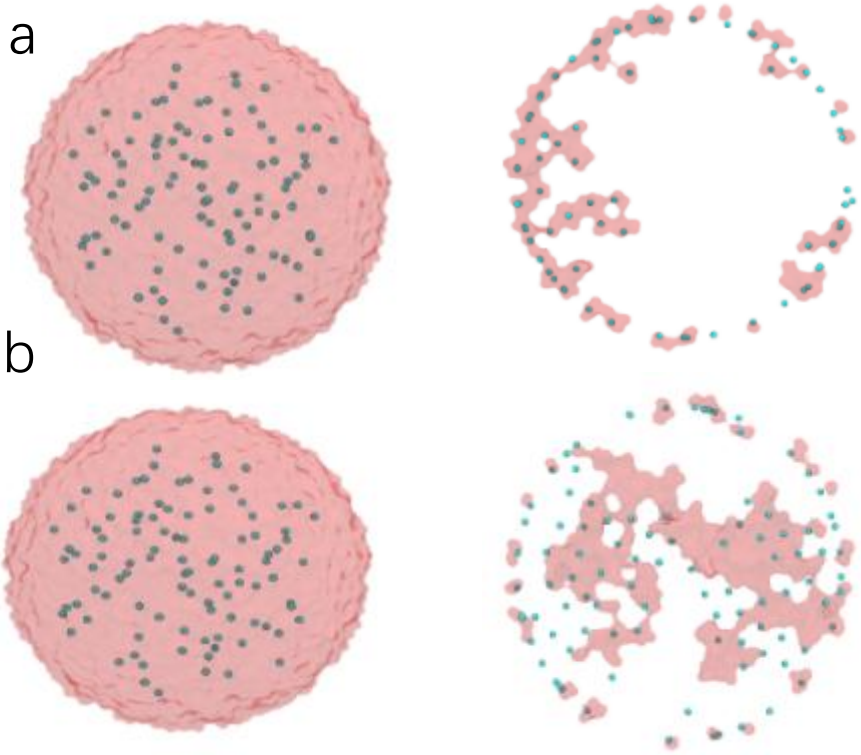

Figure S16: Series of in situ snapshots of the bottom of drops of suspension (a) or mixture (b) with different Na^+ concentrations (0 and 8.0 mM) during evaporation on transparent PET films. Arrows display the flow direction of polystyrene particles at the absence of Na^+. The t_f denotes the lifetime of evaporating drops. Scale bars are 1 mm.

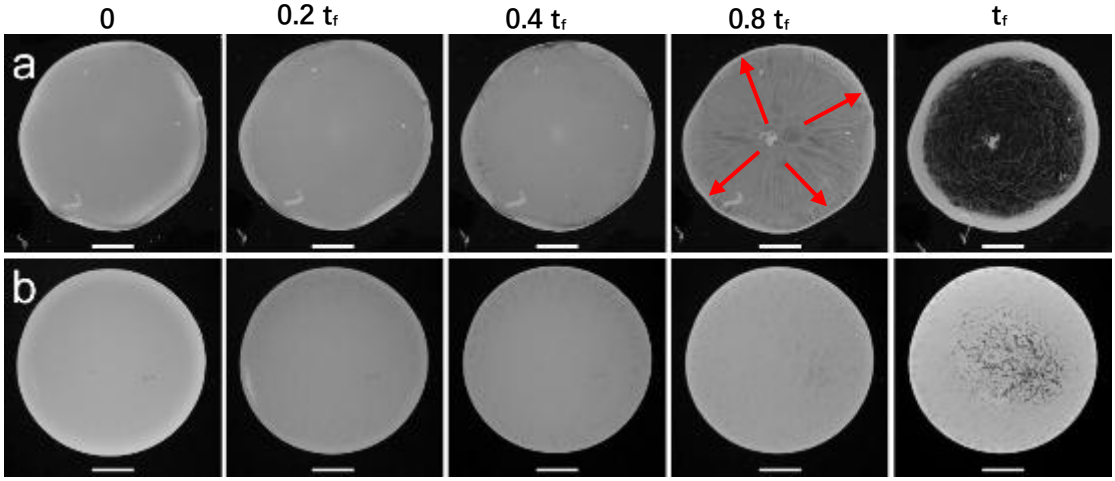

Figure S17: Deposited patterns of a drop of polystyrene microspheres containing different NaCl concentrations after evaporation on glass slides. a, 0 mM, b, 2.0 mM, c, 4.0 mM, d, 8.0 mM, e, 16 mM. Scale bars: 1mm. The typical ring-like structure exists in all these deposited patterns on glass slides, even at the NaCl concentration of 16 mM in the mixture. That is to say, cations could not suppress the coffee ring effect on substrate without aromatic rings. This contrastive experiment result reflects the key role of the cation-π interaction between the hydrated cations and aromatic rings in the surfaces in the ionic control on the coffee ring effect.

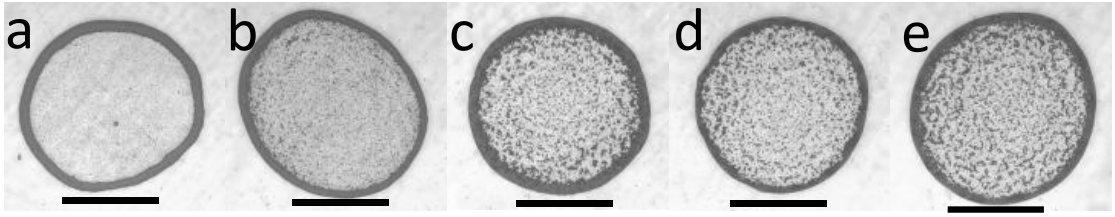

References

[1] Wang H 2017 *Science of Advanced Materials* **9** 56

[2] Yang C-W, Leung K-t, Ding R-F et al 2018 *Sci. Rep.* **8** 3125

[3] Bogdanovic G, Meurk A and Rutland M W 2000 *Colloids Surf., B* **19** 397

[4] Chen L, Shi G, Shen J et al 2017 *Nature* **550** 380

[5] Phillips J C, Braun R, Wang W et al 2005 *Journal of computational chemistry* **26** 1781

[6] Zhang J, Leroy F and Müller-Plathe F 2014 *Phys. Rev. Lett.* **113** 046101

[7] Vrbka L and Jungwirth P 2005 *Phys. Rev. Lett.* **95** 148501

[8] Nagata Y, Usui K and Bonn M 2015 *Phys. Rev. Lett.* **115** 236102

[9] Zhakhovskii V V and Anisimov S I 1997 *J. Exp. Theor. Phys.* **84** 734

[10] Wan R and Shi G 2017 *PCCP* **19** 8843

[11] Essmann U, Perera L, Berkowitz M L et al 1995 *J. Chem. Phys.* **103** 8577

[12] Shi G, Liu J, Wang C et al 2013 *Sci. Rep.* **3** 3436

[13] Wen B, Zhou X, He B et al 2017 *Phys. Rev. E* **95** 063305

[14] Wen B, Huang B, Qin Z et al 2018 *Computers & Mathematics with Applications* **76** 1686

[15] Wen B, Zhang C, Tu Y et al 2014 *J. Comput. Phys.* **266** 161

[16] Lallemand P and Luo L-S 2003 *Phys. Rev. E* **68** 036706

[17] Deegan R D, Bakajin O, Dupont T F et al 2000 *Phys. Rev. E* **62** 756

[18] Desarnaud J, Derluyn H, Carmeliet J et al 2014 *J. Phys. Chem. Lett.* **5** 890

[19] Soulié V, Karpitschka S, Lequien F et al 2015 *PCCP* **17** 22296

[20] Shahidzadeh N, Schut M F L, Desarnaud J et al 2015 *Sci. Rep.* **5** 10335